Simulations and experiments with space-charge-dominated beams[a)]

R. A. Kishek,[b)] S. Bernal, C. L. Bohn,[c)] D. Grote,[d)] I. Haber, H. Li, P. G. O'Shea,[e)] M. Reiser, and M. Walter
Institute for Research in Electronics and Applied Physics, University of Maryland, College Park, Maryland 20742-3511

(Received 18 November 2002; accepted 10 January 2003)

Beams in which space charge forces are stronger than the force from thermal pressure are nonneutral plasmas, since particles interact mostly via the long-range collective potential. An ever-increasing number of applications demand such high-brightness beams. The University of Maryland Electron Ring [P. G. O'Shea *et al.*, Nucl. Instrum Methods Phys. Res. A **464**, 646 (2001)], currently under construction, is designed for studying the physics of space-charge-dominated beams. Indirect ways of measuring beam emittance near the UMER source produced conflicting results, which were resolved only when a direct measurement of phase space indicated a hollow velocity distribution. Comparison to self-consistent simulation using the particle-in-cell code WARP [D. P. Grote *et al.*, Fusion Eng. Design **32-33**, 193 (1996)] revealed sensitivity to the initial velocity distribution. Since the beam is born with nonuniformities and granularity, dissipation mechanisms and rates are of interest. Simulations found that phase mixing by means of chaotic particle orbits is possible in certain situations, and proceeds much faster than Landau damping. The implications for using beams to model other *N*-body systems are discussed. © *2003 American Institute of Physics.* [DOI: 10.1063/1.1558291]

I. INTRODUCTION

A charged particle beam in which the repulsive space charge forces are stronger than the outward force from thermal pressure is called space-charge dominated.[1] In this regime, the Debye length is smaller than the beam size, and so particles interact mostly via the long-range collective potential, as in a (non-neutral) plasma. Whereas many emerging accelerator applications require maintaining higher beam intensities, most beams are actually created in this intensity regime near their source, but eventually the space charge forces relatively weaken due to acceleration, transverse compression, and an increase in thermal pressure caused by emittance growth. Even when space charge is not an important factor in the behavior of the bulk of an accelerator system, it can still be important to include the influence of space charge in system design. To begin with, the characteristics of the source region determine the initial state of the beam, and characteristics of the initial state such as beam emittance and halo formation[2] are often quite important to downstream behavior. Less apparent is that space-charge collective modes that persist for hundreds of focusing periods can be excited in the source region under some conditions.[3] It is therefore important to understand the effects of intense space charge on beam dynamics, since the initial beam state can affect downstream emittance growth, halo formation, and the broadening of ring resonances. The University of Maryland Electron Ring (UMER),[4] currently under construction, is designed for conducting beam physics experiments at extreme intensities in a circular lattice, and will serve as low-cost model of high-intensity accelerators for a variety of applications, such as heavy-ion fusion drivers, the low-energy end of high intensity electron linacs, ion booster synchrotrons, muon colliders, and spallation neutron sources.

Since a space-charge-dominated beam can be viewed as a one-component non-neutral plasma where the averaged focusing forces take the place of a fixed neutralizing background, it is a medium that can carry waves or collective oscillations.[5] Yet despite the fact that thermal pressure is much less than space charge forces, the beam kinetic temperature cannot be completely neglected. As we shortly present, the detailed evolution of space charge waves depends not only on the rms temperature or emittance, but also on the detailed velocity space distribution. After a brief overview of UMER in the next section, we present experimental measurements of the beam distribution function near the UMER electron gun. Various indirect methods of measurement give us conflicting results, which cannot be reconciled except by assuming a hollow velocity distribution, a fact verified by direct mapping of phase space using a pepper-pot. We augment the experimental results with self-consistent particle-in-cell simulations using the particle-in-cell code WARP, developed at Lawrence Livermore National Laboratory.[6] The beam emerging from the source is far from equilibrium, instead carrying waves and granular microstructures. We are therefore interested in dissipation mechanisms and rates and, in particular, the possibility of rapid phase mixing by means of chaotic particle orbits. An ongoing

[a)]Paper GI2 4, Bull. Am. Phys. Soc. **47**, 137 (2002).
[b)]Invited speaker. Electronic mail: ramiak@ebte.umd.edu
[c)]Northern Illinois University, DeKalb, Illinois; also Fermi National Lab, Batavia, Illinois.
[d)]Lawrence Berkeley National Laboratory, Berkeley, California.
[e)]Also at Department of Electrical and Computer Engineering, University of Maryland, College Park, Maryland.

TABLE I. UMER design specifications.

Beam energy	10 keV
$\beta\ (=v/c)$	0.2
Beam current	$\leqslant$100 mA
Generalized perveance	$\leqslant$0.0015
Emittance, 4× rms, norm	10 μm
Pulse length	40–100 ns
Ring circumference	11.52 m
Lap time	197 ns
Pulse repetition rate	60 Hz
Mean beam radius	$\leqslant$1 cm
FODO period	0.32 m
Zero-current phase advance, σ_o	76°
Zero-current betatron tune, v_o	7.6
Tune depression	$\geqslant$0.2

simulation study is highlighted in Sec. IV, and its implications are discussed.

II. OVERVIEW OF UMER

Table I lists some relevant parameters for UMER, which is discussed in more detail in Ref. 4, and on the website http://www.ireap.umd.edu/umer. The beam presently drifts at 10 keV, so the β of 0.2 implies the beam is nonrelativistic. Three induction gaps distributed equidistantly around the ring provide longitudinal focusing, and will also be used to accelerate the beam to 50 keV in a future stage. Transverse focusing is provided by 36 alternating-gradient quadrupole (FODO) cells around the 11.52 m circumference of the ring. Each pair of FODO cells, along with two 10° bends, is installed on one out of 18 mechanical sections. As of November 2002, the injector and the first four ring sections have been installed and characterized, providing data from nine bends. Additional sections are assembled and ready to be installed as part of a phased installation program. The entire ring is scheduled to be complete during the summer of 2003.

The beam intensity can be quantified in a number of ways, for example using the dimensionless intensity parameter, χ, defined as the ratio of the space-charge force to the external focusing force at the beam radius (see also Ref. 4). The space charge depresses the betatron oscillation frequency by a ratio $\omega_\beta/\omega_{\beta o}=k/k_o=\sqrt{1-\chi}$, while the plasma frequency ω_p is enhanced, $\omega_p/\omega_{\beta o}=\sqrt{2\chi}$. Another parameter of importance, which is related directly to the value of χ, is the ratio of beam radius, r_b, to the Debye length $\lambda_D=v_{\rm th}/\omega_p$, where the beam kinetic energy in a comoving frame is $\frac{1}{2}mv_{\rm th}^2$ and the plasma frequency $\omega_p^2=(4\pi ne^2/m)$, n is the particle number density, e is the particle charge, and m is the particle mass. For intensities above $\chi=0.5$, the Debye length becomes significantly smaller than the beam radius, and the beam is able to support collective space-charge oscillations, since those oscillations usually do not occur at wavelengths less than λ_D.

With the design beam current of 100 mA, an initial emittance of $\epsilon_n=12-15$ μm and a zero-current phase advance per period of $\sigma_0=76°$ (giving a beam radius $a=1$ cm), UMER can achieve an intensity of $\chi=0.97$, which is near the extreme intensity. The intensity of the UMER beam can be reduced over a wide range (down to $\chi\sim0.35$) by changing the anode–cathode spacing, the beam energy, the potential at the cathode grid, or by changing the aperture size in the beam collimator at the exit of the gun. In this paper, emittance refers to the normalized effective emittance calculated according to the formula,[1]

$$\epsilon_{xn}^2=16\beta\gamma(\langle x^2\rangle\langle x'^2\rangle-\langle xx'\rangle^2), \tag{1}$$

where the $\langle\cdots\rangle$ indicate taking the moments over the 4D transverse beam distribution $f(x,x',y,y')$. Here x is the particle position in the horizontal direction (minus the beam centroid), x' is the particle angle with the reference trajectory, v_x/v_z (minus that of the beam centroid), β is the beam velocity normalized to the speed of light, and γ is the relativistic factor. A similar expression holds for the y emittance, ϵ_{yn}.

To allow detailed comparison between theory and experiment, UMER has a comprehensive set of beam diagnostics. In addition to the 13 diagnostic stations around the ring with phosphor screens and capacitive beam position monitors (BPMs), the induction gaps will be initially operated as resistive BPMs to maximize the position data for beam steering purposes. Two fast current monitors will also be installed in the injection and extraction lines. A sophisticated diagnostic end-chamber is currently in operation and will eventually reside at the end of the extraction section. The chamber houses emittance meters of both the slit-wire and pepper-pot types; a retarding-field energy analyzer with eV or sub-eV resolution for energy and energy spread measurements;[7] a movable phosphor screen with up to 1.5 m travel for insertion into the extraction transport line; and a Faraday cup for current measurement. Charge-coupled device (CCD) cameras record the time-integrated images of the beam from the phosphor screens.

III. SIMULATING SOURCE AND INJECTOR EXPERIMENTS

A. Simulation code and model

The simulations presented here employ the particle-in-cell code WARP (Ref. 6) to self-consistently simulate space charge effects in our experiments. The WARP code simulates space charge effects in 2D or 3D by advancing a large number of macroparticles in response to both the external applied fields and the self-fields. The self-fields are calculated on a mesh of sufficient resolution to capture the variations of the beam potential, and the particles are advanced using a leap-frog algorithm. WARP has been under development for nearly a decade, so it possesses a variety of models for various accelerator elements—magnets, induction gaps, apertures, etc.—as well as many different choices of field solvers, boundary conditions, and numerical algorithms. Many input beam distributions are also possible, of which the most commonly used for space-charge-dominated beams is the semi-Gaussian, in which the particle density is uniform across the beam, while the velocity distribution is Gaussian with uniform temperature.

Although most of the simulations reported here were modeled with the 2-1/2 D ''slice'' version of WARP (WARPxy), which solves for the transverse behavior while

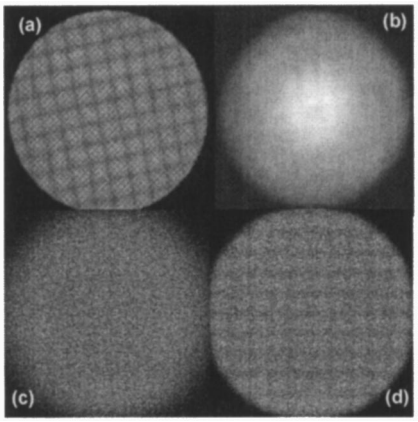

FIG. 1. Photographs of (a) cathode (fine) and anode (coarse) grids without the beam; (b) beam incident on phosphor screen 6 cm downstream from anode grid, exhibiting a shadow of the anode grid; (c) simulation of (b) using semi-Gaussian distribution with 12 μm emit; and (d) same simulation with 4 μm emit.

advancing a beam slice along *s*, some problems are inherently three-dimensional. The source simulations employed the $r-z$ axisymmetric module, which is also used for modeling propagation and confinement of the beam ends and the retarding voltage energy analyzer.

B. The UMER electron gun

The electron gun is of Pierce geometry with a 4 mm radius cathode.[8] Changing the A/K separation or the grid-cathode potential can vary the perveance. Since the accelerating potential across the gap is applied using a dc 10 kV power supply, a grid located 0.15 mm from the cathode surface is biased negatively (usually at 40–50 V) in order to impede the current flow until a positive pulse is applied to the grid. Since the separation between the wires in the rectangular grid pattern is 0.15 mm, i.e., the same as the distance to the cathode, the field pattern in the vicinity of the emitter surface is complex, especially when beam space charge is included. Another grid (with 87% transmission and a wire spacing of 0.69 mm) intercepts the beam in the anode plane in order to create an equipotential surface, as E-GUN simulations had shown this method reduces gun aberrations. The grids appear in a photograph taken without the beam [Fig. 1(a)]. In addition, the UMER gun structure has a set of masks on a plate that can be rotated without breaking vacuum. This mask plate contains a pepper-pot mask for measuring transverse phase space, a five-beamlet quincunx pattern (similar to the five on the face of a die), as well as a series of round holes with various radii used to change the beam current and emittance to provide beams with widely different intensities.

C. Measurement of the initial beam distribution

1. Shadow of anode grid

One of the early mysteries in characterizing the UMER gun was estimating the emerging beam's emittance. A calculation of intrinsic emittance provides a value of 3.6 μm, given the cathode radius and cathode temperature measured

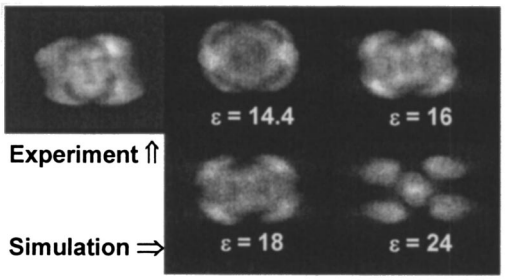

FIG. 2. Photograph of beam incident on a phosphor screen 104 cm downstream from the anode while the five-beamlet mask is applied near the anode. The experiment is compared with the results of four simulations starting with a semi-Gaussian distribution at the anode, but with different initial emittances, marked on the figures.

by a pyrometer.[8] This number, however, proved inconsistent with *some* of the measurements. For example, the beam size from transport experiments in the injector hinted at a much larger emittance (~12–15 μm). The interesting issue is that a P-screen positioned 6 cm downstream from the anode clearly shows a shadow of the anode grid pattern,[9] as in Fig. 1(b). WARP*xy* simulations using the slice model and an initial semi-Gaussian distribution starting from the anode with the higher emittance have been unable to reproduce the grid pattern [Fig. 1(c)], as the shadow tends to wash out very quickly. Yet when the simulation emittance is reduced to near the intrinsic emittance, the grid shadow pattern can be seen in the simulation [Fig. 1(d)].

2. Five-beamlet merging

The emittance mystery compounded with additional data. Figure 2 shows phosphor screen images measured 104 cm downstream from the anode plane when the five-beamlet mask is used. This photograph is typical of the whole series of pictures taken along the injector using the moveable P-screen. Also shown on the same figure are simulations performed using the WARP PIC code in single slice mode.[10] The emittances labeled on the simulation curves shown in Fig. 2 are calculated by multiplying the thermal velocity assumed for the beamlets by the total area the beam would have at the anode plane in the absence of the mask. It is clear that the shape of the pattern downstream depends on the beam emittance. From a comparison between the simulated and measured pattern one infers that the best match occurs when the initial normalized emittance of the total beam is between 16–18 μm. This value is a factor of 4 or 5 larger than intrinsic emittance and the near-laminar flow that would allow the shadow of the grid to persist for 6 cm.

3. Pepper-pot measurements and hollow velocity distribution

No satisfactory explanation for this behavior is possible with the simple semi-Gaussian model. Fortunately, we were able to directly measure the beam phase space using a pepper-pot mask built into the aperture wheel near the anode. The results, of which one photograph is shown in Fig. 3(a), provide the major clue for resolving this mystery. The beamlets emerging from the 0.1 mm holes in the pepperpot ex-

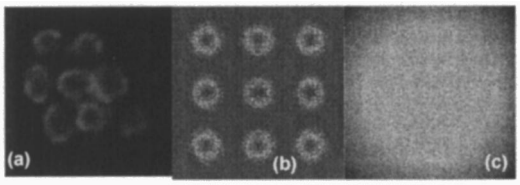

FIG. 3. (a) Pepper-pot snapshot of phase-space at gun exit, taken with the phosphor screen 6 cm downstream from pepper-pot mask near anode and a cathode-grid biased at 45 V; (b) simulation of pepper-pot starting with a annular-Gaussian distribution; and (c) simulation of grid shadow with annular-Gaussian [cf. Fig. 1(b)]. Note that the pepper-pot holes are staggered in the experiment, but lie on a square grid pattern in the simulation.

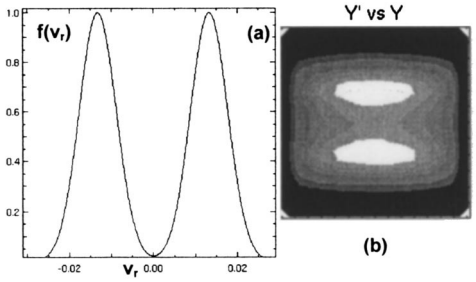

FIG. 4. The annular-Gaussian velocity distribution (a) the velocity distribution in a cross section $f(v_r)$; (b) a projection of the initial distribution on the $y-y'$ trace space.

pand to produce hollowed projections on the screen. These donuts indicate a hollowing of the *velocity space* of the beam, possibly caused by the distortion of the potential near the cathode by the (cathode) grid. Reproducing the pattern in the simulations is not simple, due to the 3D nature of the problem and the disparity of scales between the cathode grid dimensions and the A/K gap, making simulation difficult.[11] Nevertheless we were able to obtain an approximation of this effect by injecting a beam with an artificially hollowed velocity distribution into the slice code simulations at the anode. Various implementations of hollowness have been attempted, for instance one with rectangular symmetry to mimic the hollowness that could be created by the cathode grid. The results shown in the remainder of this paper use a radially hollowed velocity (i.e., possessing azimuthal symmetry) that is obtained by rotating a Gaussian distribution with width v_{th} and offset α from the origin around a circle of radius α. The cross section of such a velocity distribution on the v_x axis is shown in Fig. 4,[12] along with a snapshot of the $y-y'$ trace space. Henceforth, we refer to this distribution as ''annular-Gaussian,'' noting that the density distribution is uniform as in the semi-Gaussian.

The parameters α and v_{th} are obtained empirically by fitting to experimental data. For this paper, we use a width for the Gaussian corresponding to the intrinsic emittance, and a radius of rotation α selected to result in an rms beam emittance of 14 μm. These parameters can be varied of course, considering the pepper-pot images in the experiment itself change with the bias voltage of the cathode grid. A simulation of the pepper-pot with this distribution [Fig. 3(b)] results in a picture qualitatively similar to the experiment. Furthermore, this distribution reproduces both the shadow of the grid [Fig. 3(c)] and the five-beamlet experiment, as well as the injector experiments.

Similarly by using $r-z$ simulations of the gun structure starting from, but not including the cathode grid,[11] we were able to reproduce the experimentally measured features only when hollowness in the velocity space of the injected distribution was assumed. The agreement using the $r-z$ code was significantly better in some respects, but the point here is that even a crude 2D model with a hollowed velocity can qualitatively explain experimental features that cannot be explained with a semi-Gaussian.

D. Propagation in the injector

Figure 5(a) shows a series of beam photographs taken along the injector using a moveable P-screen.[13] The photo-

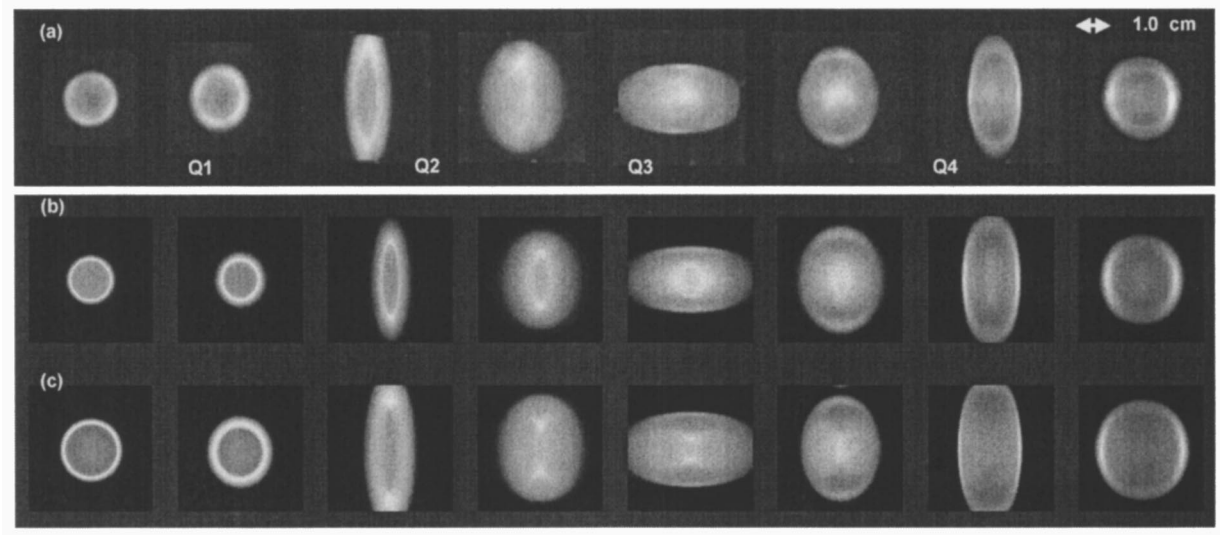

FIG. 5. Photographs of beam cross section along the injector, at 33, 39, 50, 55, 61, 67, 71, and 103 cm from the anode plane: (a) experiment; (b) simulation with semi-Gaussian distribution; and (c) simulation with annular-Gaussian distribution.

graphs demonstrate evolution of the beam as it propagates through the matching system, and exhibits space charge waves similar to one discovered in previous experiments.[14] In addition, the experimental photographs exhibit some fine-structured patterns that were not observed in the previous experiments. Since the primary difference from the earlier experiments is the added presence of the grids in the gun, we suspect that to be the main factor resulting in this fine structure. Simulations with WARP*xy* [Figs. 5(b), 5(c)], using initially uniform density distributions, but two different velocity distributions having the same rms values, demonstrate a resulting difference in the detailed density distribution downstream. In particular, the annular-Gaussian distribution used earlier [Figs. 3(c) and 4] more closely resembles the experimental results, although the agreement is not exact.

The emerging conclusion is that beam dynamics in an accelerator can be very sensitive to the details of the 6D distribution at the source. Even if a beam appears to be well-behaved in configuration space, distortions in velocity space can reappear as density structures later downstream. Note that this fine structure persists for a long time. In our case the hollowness in the velocity distribution caused by the cathode grid persists as fine structure in the beam even in the latest experimental photographs 9 bends past the injector, i.e., several plasma periods from the cathode. While the rms beam size and other second order moments are affected only by the rms emittance as calculated in Eq. (1), it is clear that the detailed density patterns including the propagation and phases of space charge waves are affected by the higher-order moments of the initial distribution. As we have shown, it is possible to construct two completely different distributions with identical emittances, such as a thermal distribution and one with two laminar ''streams'' propagating at an angle to each other, but obviously the beam dynamics will evolve differently for the different distributions when the details are considered.

IV. STUDIES OF MIXING BY MEANS OF CHAOTIC ORBITS

A related issue, of fundamental importance to beam physics as well as plasma physics in general, is mixing and dissipation of charge density structures and granularities, such as those we measured in the UMER beam near the source. Beams with space charge are, like many plasmas, typically collisionless Hamiltonian systems where the detailed density distribution self-consistently governs the dynamics via Poisson's equation. The questions of equilibration, damping, and reversibility are of fundamental importance in determining beam properties. For example, equipartitioning of anisotropic beams involves nonlinear energy transfer and evolution towards an isotropic meta-equilibrium.[15] It is important for the accelerator designer to know whether the exchange of energy in this process is reversible. Another example, while it may be possible to correct for emittance growth in a 3D context by emittance compensation techniques,[16] this compensation needs to be applied before any significant mixing has rendered the growth irreversible. The same question arises when considering any process manipulating a space charge-dominated beam; whether it is flat beam generation, bunch distortion due to coherent synchrotron radiation, matching through transitions in a linac, or emittance growth due to misalignments or dispersion. Furthermore, these issues are of importance beyond the plasma or beams community, as they apply to any N-body system interacting via long-range forces without collisions, as is the case in large stellar systems,[17] for example.

In order to answer these questions we are conducting a large-scale simulation study of beam dynamics with a focus on individual particle orbits.[18] Whereas traditional PIC simulation is concerned mostly with the macroscopic behavior resulting from the interaction of macroparticles, we require sufficient numerical resolution so as to observe reliable macroparticle orbits and analyze them statistically. Our main concern is whether or not particles follow globally chaotic orbits, i.e., mix chaotically until they fill their total accessible phase space, in which case they can phase mix quite rapidly at rates that can be calculated from theory.[19]

To determine this, we seed large numbers of test particles concentrated in various locations in 4D phase space. The remainder of the beam should have a sufficient number of particles and sufficiently fine simulation mesh to produce a smooth and well-resolved potential at every step. Time steps are chosen small enough relative to the natural frequencies of the system to result in a sufficiently smooth trajectory. Particle advance is done using a symplectic leap-frog algorithm, which guarantees that the numerical simulation itself is reversible. Tracking the test particles in the self-consistent potential of the beam, we then look for exponential separation of orbits indicative of chaos, in which case we can calculate the finite-time Lyapunov exponents[20] for each initially localized collection of test particles. Note that since in general we do not have equilibrium, the problem is time dependent. An example is shown in Fig. 6[12] comparing the ''emittance'' moments for five clumps of test particles [defined as in Eq. (1), but including only particles belonging to a particular clump] for each of two test cases: a round isotropic space-charge-dominated beam in a uniform focusing channel, and an otherwise similar beam having different initial emittances (hence temperatures) in x and y. The anisotropic case has been observed to macroscopically relax to an isotropic beam on a very fast time scale (2–3 plasma periods).[15] The mixing rate, defined as the growth rate of the ''emittance'' moment of each clump (indicative of the separation of nearby trajectories), proceeds much faster for the anisotropic beam, as evident from Fig. 6. Furthermore, this growth for the anisotropic beam fits closely to a straight line on a semi-log plot, indicating exponential growth. A comparison of trajectories in $x-z$ space of 20 sample test particles from one clump in each case indicates a qualitative difference in behavior (Fig. 7).

The fundamental significance of this type of study is that chaotic mixing can be found in many types of physical systems. Whereas large stellar systems are largely inaccessible outside of computer simulations, beam experiments can nevertheless be constructed to test hypotheses pertaining to fundamental questions in galactic dynamics.

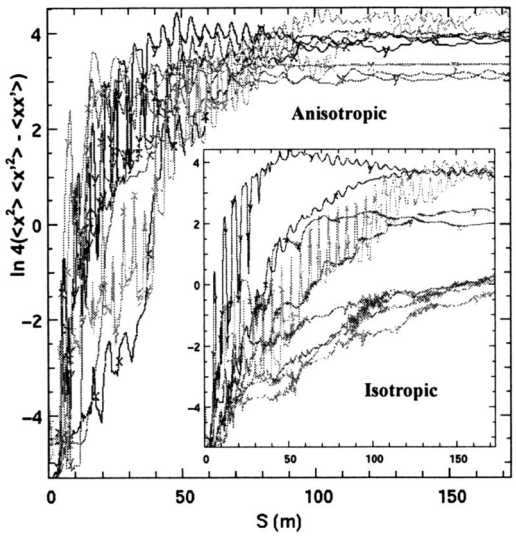

FIG. 6. Evolution along the beamline of the natural logarithm of x and y ''emittance moments'' for 5 color-coded ''clumps'' of test particles launched in an initially anisotropic beam with $\epsilon_x = 2\epsilon_y$, and an average intensity $\chi = 0.96$. The inset shows the same plot for an initially isotropic beam (i.e., $\epsilon_x = \epsilon_y$) with otherwise similar parameters.

V. CONCLUSION

Measurements of the space-charge-dominated beam in the UMER source and injector have been compared to self-consistent particle-in-cell simulations using the WARP code. The various indirect measurements exhibit mutual contradiction in the inferred value of emittance if a semi-Gaussian distribution is assumed. This contradiction has been removed once a direct measurement of phase space using a pepper-pot identified a hollowed velocity distribution. Even an *ad hoc* use of a hollowed velocity distribution in the simulations resulted in much-improved agreement with experimental results. This emphasizes the indispensability of direct phase space measurements, as well as demonstrates the sensitivity of detailed beam distributions downstream to the velocity distribution at the source.

Dissipation of granularities and microstructures such as what has been observed in the experiment has also been studied using the WARP simulations. Results indicate rapid mixing by means of chaotic particle orbits can take place in certain circumstances. This raises the possibility of setting up charged particle beam experiments to model other and less-accessible N-body systems such as galaxies.

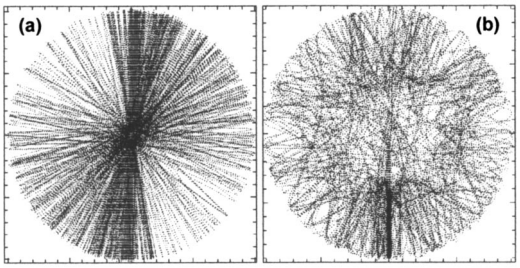

FIG. 7. Trajectories of 20 test particles in x–y space from one typical clump in (a) the isotropic beam and (b) the anisotropic beam.

ACKNOWLEDGMENTS

We wish to acknowledge David Kehne and FM Technologies, Inc., for the design and construction of the gun and diagnostic chamber. We are also grateful for many productive discussions with David Kehne, Alex Friedman, Henry Kandrup, Tom Antonsen, Steve Lund, Jean-Luc Vay, Ioannis Sideris, as well as other members of the UMER team.

This work is performed under the auspices of the U.S. Department of Energy under Contracts Nos. DEFG02-94ER40855, DEFG02-92ER54178, W-7405-Eng-48, and DE-AC03-76SF00098, as well as a Department of Education, NICADD grant.

[1] M. Reiser, *Theory and Design of Charged Particle Beams* (Wiley, New York, 1994).
[2] T. P. Wangler, K. R. Crandall, R. Ryne, and T. S. Wang, Phys. Rev. ST Accel. Beams **1**, 084201 (1998).
[3] S. M. Lund and R. C. Davidson, Phys. Plasmas **5**, 3028 (1998).
[4] P. G. O'Shea, M. Reiser, R. A. Kishek *et al.*, Nucl. Instrum. Methods Phys. Res. A **464**, 646 (2001); ''Experiments with space charge dominated beams for heavy ion fusion applications,'' Laser Part. Beams (in press).
[5] R. C. Davidson and H. Qin, *Physics of Intense Charged Particle Beams in High Energy Accelerators* (World Scientific, Singapore, 2001).
[6] D. P. Grote, A. Friedman, S. M. Lund, and I. Haber, Fusion Eng. Des. **32-33**, 193 (1996).
[7] Y. Zou, Y. Cui, V. Yun, A. Valfells, R. A. Kishek, S. Bernal, I. Haber, M. Reiser, P. G. O'Shea, and J. G. Wang, Phys. Rev. ST Accel. Beams **5**, 072801 (2002); Y. P. Cui, S. Bernal, R. A. Kishek *et al.*, ''Design studies for an experiment to measure energy spread evolution through a solenoidal focusing system,'' in *Proceedings of the 2001 Particle Accelerator Conference, Chicago, IL, 2001*, edited by P. Lucas and S. Weber (IEEE, Piscataway, NJ, 2001), I4 Cat. No. 01CH37268, p. 2976.
[8] D. Kehne, T. Godlove, P. Haldemann *et al.*, Nucl. Instrum. Methods Phys. Res. A **464**, 605 (2001).
[9] We can tell the pattern results from the anode grid rather than the cathode grid because the two grids are oriented at different angles.
[10] I. Haber, F. M. Bieniosek, C. M. Celata *et al.*, ''End-to-end simulation: The front end,'' Laser Part. Beams (in press).
[11] I. Haber, S. Bernal, C. M. Celata, A. Friedman, D. P. Grote, R. A. Kishek, B. Quinn, P. G. O'Shea, M. Reiser, and J.-L. Vay, ''Collective space-charge phenomena in the source region,'' Nucl. Instrum. Methods Phys. Res. A (submitted).
[12] See EPAPS Document No. E-PHPAEN-10-924305 for color versions of Figs. 4 and 6 of this paper. A direct link to this document may be found in the online article's HTML reference section. The document may also be reached via the EPAPS homepage (http://www.aip.org/pubservs/epaps.html) or from ftp.aip.org in the directory /epaps/. See the EPAPS homepage for more information.
[13] S. Bernal, B. Beaudoin, Y. Cui *et al.*, ''Intense beam transport experiments in a multibend system at the University of Maryland Electron Ring (UMER),'' Nucl. Instrum. Methods Phys. Res. A (submitted).
[14] S. Bernal, R. A. Kishek, M. Reiser, and I. Haber, Phys. Rev. Lett. **82**, 4002 (1999); S. Bernal, B. Quinn, P. G. O'Shea, and M. Reiser, Phys. Rev. ST Accel. Beams **5**, 064202 (2002).
[15] R. A. Kishek, P. G. O'Shea, and M. Reiser, Phys. Rev. Lett. **85**, 4514 (2000).
[16] B. E. Carlsten and D. T. Palmer, Nucl. Instrum. Methods Phys. Res. A **425**, 37 (1999).
[17] H. Kandrup, I. Pogorelov, and I. Sideris, Mon. Not. R. Astron. Soc. **319**, 43 (2000).
[18] R. A. Kishek, C. L. Bohn, I. Haber, P. G. O'Shea, M. Reiser, and H. Kandrup, in *Proceedings of the 2001 Particle Accelerator Conference, Chicago, IL, 2001*, edited by P. Lucas and S. Weber (IEEE, Piscataway, NJ, 2001), I4 Cat. No. 01CH37268, p. 151.
[19] C. L. Bohn, in *The Physics of High Brightness Beams*, edited by J. Rosenzweig and L. Serafini (World Scientific, Singapore, 2000), p. 358.
[20] T. Antonsen, Fan, E. Ott, and Garcia-Lopez, Phys. Fluids **8**, 3094 (1996).